An Implicit Study of High Order Elements in LS-DYNA

Thomas Borrvall[1], David Benson[2], Hailong Teng[2]

[1]DYNAmore Nordic AB, Linköping, Sweden
[2]LSTC, Livermore, CA, USA
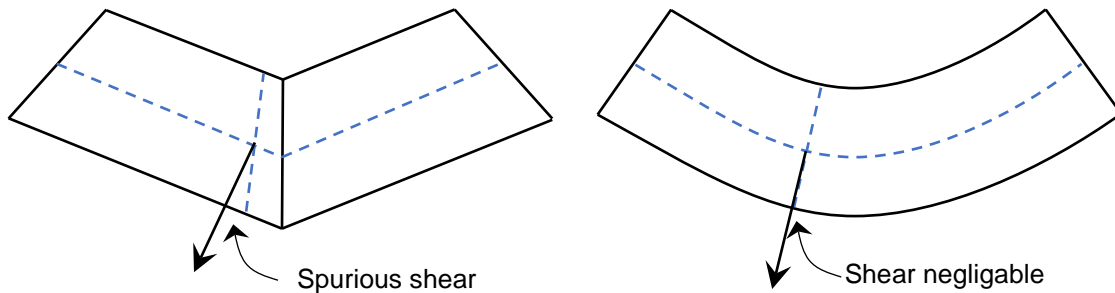
Figure 1 High order elements tend to alleviate spurious shear deformation in bending, for pure bending the shear is exactly zero in the center of the elements. The latter observation is taken advantage of in the 6-noded shell.

1 Introduction

High order elements have always been of interest in linear finite element analysis. The primary reason is that mesh convergence rate is proportional to the polynomial order of the isoparametric shape functions used, see for instance Hughes [2]. An intuitive understanding can be obtained through the illustration in Figure 1; basically the deformation space of low order elements is restricted to the extent that pure bending will inevitably induce spurious transverse shear and result in a locking phenomenon. Even though this anomaly is present in high order elements, the effect is significantly reduced with increasing polynomial order.

For decades, LS-DYNA [1] was developed with sole emphasis on explicit dynamic analyses. Computational efficiency of the involved model features, element formulations in particular, has therefore been of uttermost importance. In this context, the compromise between efficiency and accuracy has made low order elements the preferred choice while high order elements have been pushed down the priority list. The last few years, owing to a number of factors including the desire for more accuracy, improved computer technology, and an increasing use of implicit analysis, tables have turned. Users are more open to pay the price of longer simulation times with better results in return. This is true not only for implicit analysis; in explicit crash, high order elements may be required to capture the stress response necessary for assessing failure of critical components.

The present paper has focus on implicit analysis of high order shells and solids, with the intention to give an overview of the current state of the LS-DYNA capabilities in this area. Sections 2 and 3 provide theories of high order shells and solids, respectively, together with some examples and discussion. In Section 4, a description of the consistent contact treatment is given, according to the implementation of the Mortar contact in LS-DYNA, and the paper ends with a summary and outlook in Section 5.

2 Quadratic Shells
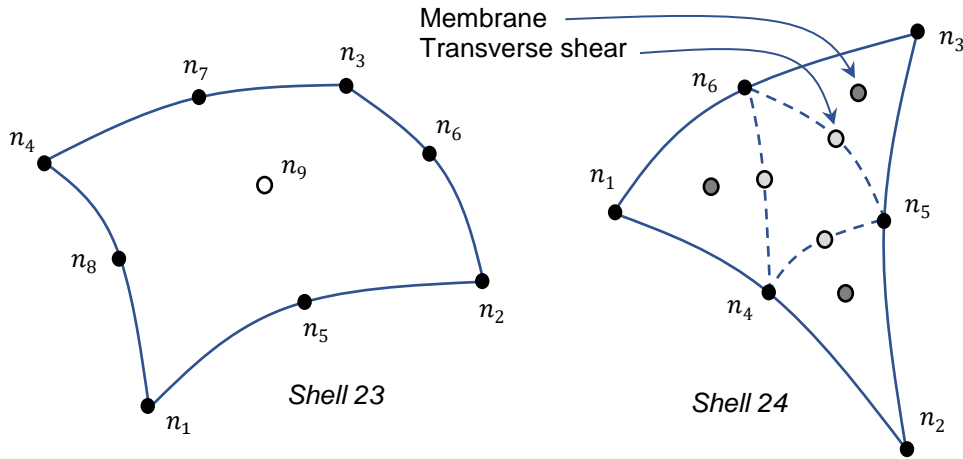
Figure 2 Quadratic quadrilateral and triangle, including a virtual node for contact (n_9). Membrane and transverse shear integration points for the 6-noded shell are indicated.

2.1 Theory

The quadratic quadrilateral and triangular elements in LS-DYNA are of serendipity type and illustrated in Figure 2. In the following, Section 2.1.1 pertains to both shell types, whereas Section 2.1.2 largely follows the MB6 formulation in [3] and is only implemented for the 6-noded shell and implicit.

2.1.1 Isoparametric representation

The shape functions N_I, $I = 1,2,..,n$, are standard, where $n = 6$ for the triangle and $n = 8$ for the quadrilateral, and the isoparametric representation is given as (sum over I)

$$x = x_I N_I(\xi, \eta) + \zeta \frac{t}{2} n(\xi, \eta),$$

where x_I are the nodal coordinates and t is the thickness of the shell (assumed constant). The normal to the shell at any point is given as $n = m/|m|$ where

$$m = \frac{\partial x}{\partial \xi} \times \frac{\partial x}{\partial \eta}$$

at ζ=0. Following a standard procedure, the velocity gradient in local coordinates can be expressed as

$$\frac{\partial v}{\partial x} = \left[\frac{\partial v}{\partial x_\alpha} \quad \frac{\partial v}{\partial z} \right]$$

and

$$\frac{\partial v}{\partial x_\alpha} = v_I \frac{\partial N_I}{\partial x_\alpha} + z \left\{ \left(\omega_I \frac{\partial N_I}{\partial x_\alpha} \right) \times n + (\omega_I N_I) \times \frac{\partial n}{\partial x_\alpha} \right\}$$

$$\frac{\partial v}{\partial z} = (\omega_I N_I) \times n$$

where v_I and ω_I are the nodal translational and rotational velocities, respectively, and the subscript α indicates the in-plane coordinates.

2.1.2 Membrane and transverse shear locking

According to Martin et.al. [3], even quadratic shells suffer from membrane and transverse shear locking, and they present approaches to overcome these deficiencies.

For the membrane locking they substitute the membrane part of the strain-displacement matrix $\boldsymbol{B}_i$, $i = 1,2,3$, for

$$\widetilde{\boldsymbol{B}}_i = \sum_{j=1}^{3} w_j \boldsymbol{B}_j + \boldsymbol{B}_i^* - \frac{1}{3} \sum_{j=1}^{3} \boldsymbol{B}_j^*$$

where $\boldsymbol{B}_1^*$, $\boldsymbol{B}_2^*$ and $\boldsymbol{B}_3^*$ are the membrane strain-displacement matrices of the flat triangles between nodes $\{n_1, n_4, n_6\}$, $\{n_2, n_5, n_4\}$ and $\{n_3, n_6, n_5\}$, respectively, and $w_i, i = 1,2,3$, are the integration point weights.

To alleviate shear locking, they derive an assumed transverse shear strain field for which the details can be found in [3]. Unfortunately, this rather complex approach left us with a singular deformation mode that could not be reconciled, whence a simple and intuitive idea based on ANS (assumed natural strain) was employed. Referring to Figure 1 and Figure 2, the transverse shear strains are evaluated at the edges of the mid sub-triangle instead of at the standard Gauss point locations. The reason is primarily because this is a location where the direction of shell normal and through-thickness fiber coincide for pure bending and should therefore suppress spurious shear strains.
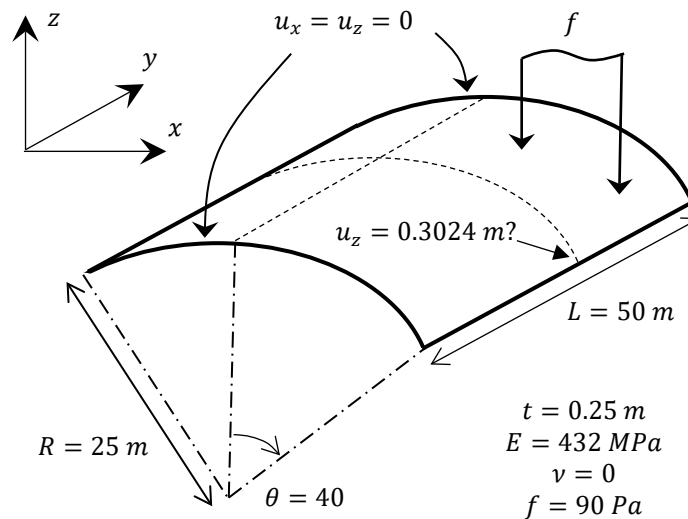
Figure 3 The Scordelis-Lo roof.

2.2 Scordelis-Lo roof

The Scordelis-Lo roof, see Figure 3 for the definition, is a standard test example for validating a shell element implementation, named after the authors who invented it. A uniform gravity load should cause a $0.3024\,m$ deflection of the mid-point of the free edge, and this example can be used to the assess the mesh convergence in linear implicit analysis. From [3], and our own observations, it is primarily the spurious membrane strain for curved geometries that prevents the roof from deflecting. The results in Figure 4 show that the attempt for alleviating this locking phenomenon has a positive impact of the overall mesh convergence[1]. The modification of transverse shear strain has a negligible influence of these results, but our next example will show the importance of that contribution.

2.3 Three Point Bending

To assess the shear locking, an elastic-plastic bending of a front bumper beam was conducted as shown in Figure 5. Five different meshes, using roughly the same number of nodes, for the beam was used; a low order quadrilateral mesh (type 16 shell), a low order triangular mesh (type 4 shell), a high order quadrilateral mesh (type 23 shell) and two high order triangular meshes (type 24 shell). The two triangle meshes used a straightforward isoparametric formulation and one with the attempt to alleviate locking phenomena. The resulting contact forces are shown in Figure 6.

---

[1] It should be mentioned that the results in [3] are much better, but we were not able to achieve those.
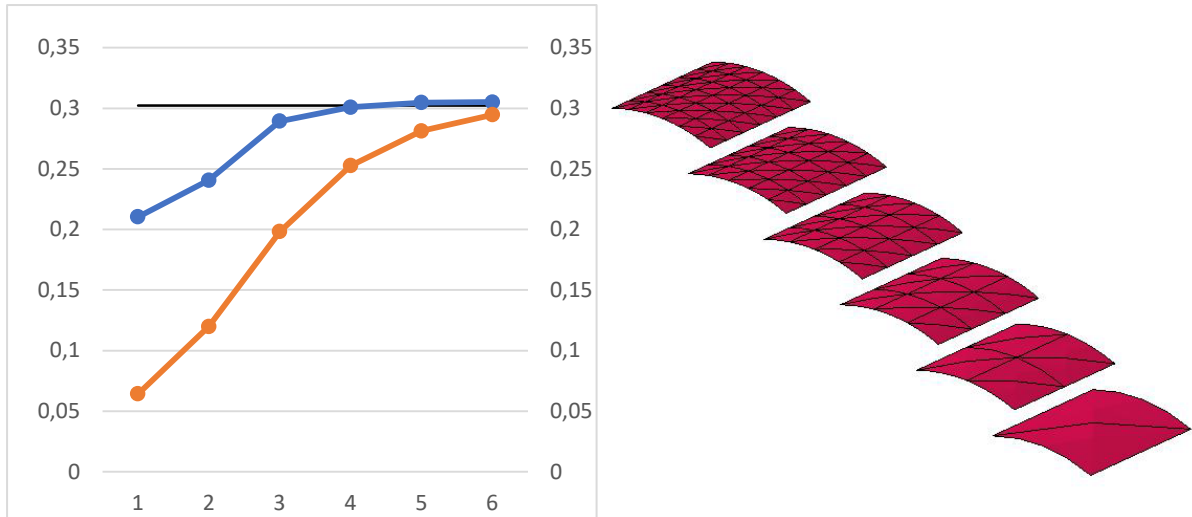
Figure 4 Mesh convergence for the Scordel-Lo roof, comparing the isoparametric approach vs alleviation of membrane and shear locking.
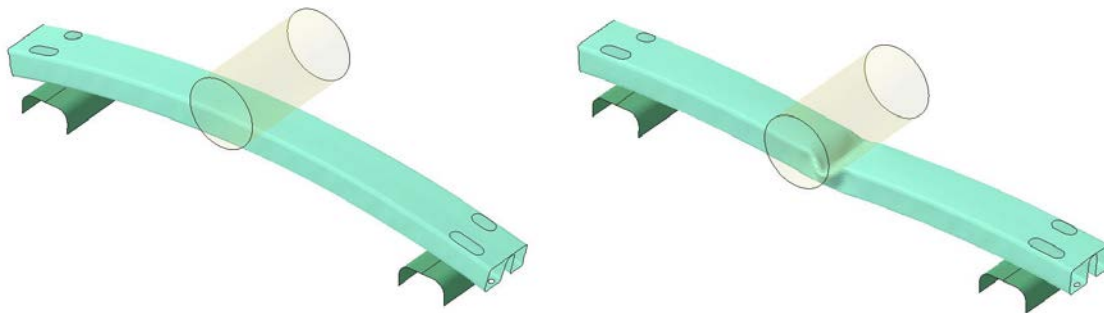
Figure 5 3-point bending of a bumper beam.
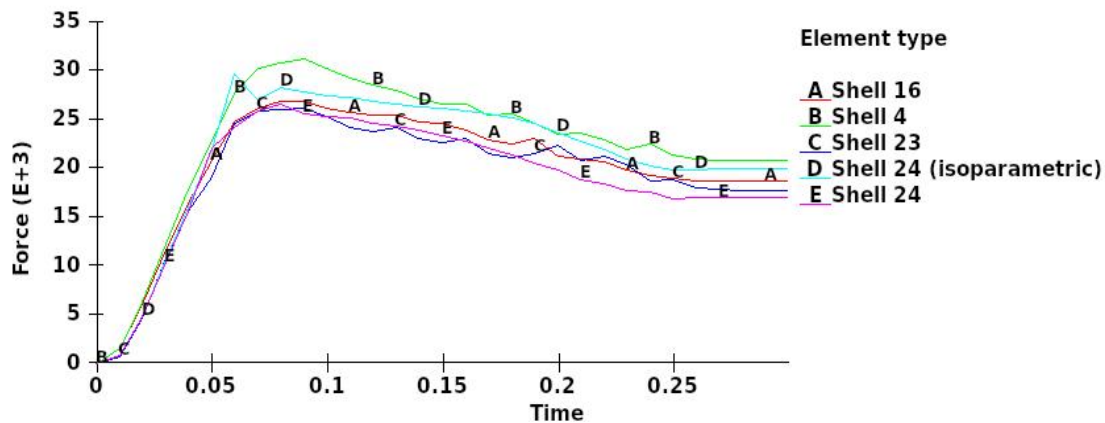
Figure 6 Contact forces for bumper beam example.

Even though it is hard to observe from the figure, the following can be noted from inspection. The initial stiffness (elastic) of the beam is considerably higher for low order triangle (curve B) and the high order triangle without any special treatment (curve D). The other are comparable, except for the high order quadrilateral being somewhat softer (curve C). The same can be said for the peak load, curves B and D stands out while the others are of the same magnitude. The residual force differs among all elements, and the high order triangle with locking treatment has the lowest force (curve E), followed by the high order quadrilateral (curve D). The other triangles are giving the stiffest response. This,

together with further observations from other runs, indicate that the locking treatment of the high order triangle is indeed providing a response that is comparable to that of quadrilateral shell elements.

Solid 23/24   *Solid ?/25*   *Solid 16/26*
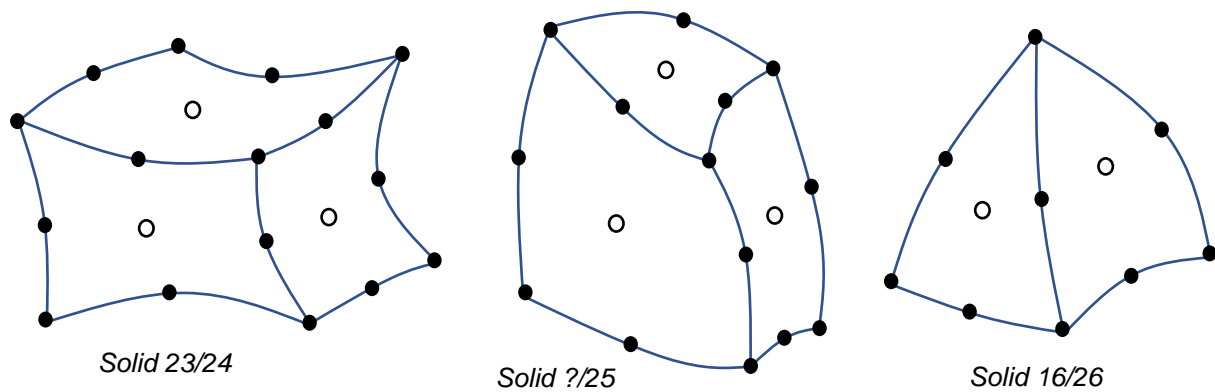
Figure 7 Quadratic hexahedron, pentahedron and tetrahedron, node numbers omitted.

3 Quadratic Solids

There are in principle two families[2] of quadratic solid elements, a serendipity family and a fully integrated family. The families are illustrated in Figure 7, where serendipity elements have corner and side nodes while the fully integrated family also have face and body nodes. Only the visible nodes are shown in the picture, out of which the face nodes are indicated by circles. Currently the serendipity pentahedron does not exist in LS-DYNA but needs to be added to complete the family, whence we focus on the fully integrated elements in the following.

3.1 The $\overline{B}$-approach

Most of the quadratic solids are iso-parametric elements adopting the conventional second order shape functions, the exception is the 27-noded solid element which is equipped with a $\overline{B}$ (B-bar) method to reduce volumetric locking. Following Hughes [2], the dilatational terms of the strain-displacement matrix $\boldsymbol{B}_I$, $I = 1,2,\ldots,27$, are interpolated as

$$\overline{\boldsymbol{B}}_I = N_J \widetilde{\boldsymbol{B}}_{JI}$$

with $\widetilde{\boldsymbol{B}}_{JI}$ obtained by the projection

$$\int N_I N_J dV \, \widetilde{\boldsymbol{B}}_{JK} = \int N_I \boldsymbol{B}_K dV$$

and integrals are over the element domain V. The projection needs to be explained further; the element itself has 27 integration points, but the integrals in the projection is performed using a Gaussian quadrature of only 8 integration points. This is the key to alleviate the locking tendencies.

The one unattractive aspect of this approach is the cost of forming and solving the projection equations. The matrix $\boldsymbol{M}$, represented by its components $M_{IJ} = \int N_I N_J dV$, depends on the geometry of the element and thus needs to be recalculated and factorized each time the geometry changes. For incompressible deformation, however, $\boldsymbol{M}$ can be assumed constant and the resulting $\overline{\boldsymbol{B}}_I$ matrix is conveniently expressed as

$$\overline{\boldsymbol{B}}_I = N_J M_{JK}^{-1} \int N_K \boldsymbol{B}_I dV$$

where M_{JK}^{-1} now are the components the inverted *initial* projection matrix, which allows for a more efficient implementation scheme. The latter integral is also simplified to be with respect to the initial

---

[2] A familiy consists of a hexahedron, a pentahedron and a tetrahedron.

configuration to avoid the dependency of the jacobian. Thus, in the context of numerical integration, the expression for $\bar{B}_I$ reads

$$\bar{B}_I(\xi_i) \approx N_J(\xi_i) M_{JK}^{-1} \sum_{j=1}^{8} N_K(\xi_j) B_I(\xi_j) V_0^j = \sum_{j=1}^{8} w_{ij} B_I(\xi_j), \quad i = 1,2,\dots,27$$

where w_{ij} can be interpreted as extrapolation weights from the reduced integration points to the full integration points. The incompressibility assumption makes sense, since this is the justification for the $\bar{B}$ method in the first place. For compressible materials, the $\bar{B}$ method can and should probably be avoided.
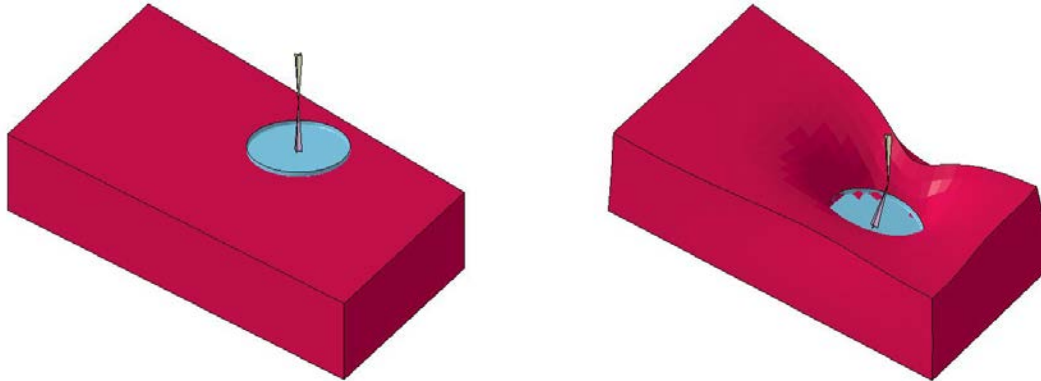
Figure 8 Initial and final configuration of foam block.

3.2   Indentation of a foam block

As a first indication of the response of quadratic solids, consider the indentation of a foam block as illustrated in Figure 8. The bottom of the block is entirely fixed as an indenter compresses the block a fair amount. The material used is a simple Fu-Chang foam without any rate or hysteresis effects and a compression curve giving the foam its characteristic properties. Figure 9 shows the input curve together with an indication of the different deformation phases.

Element	Force
2	3.70
10	4.25
24	3.51
25	3.54
26	3.96
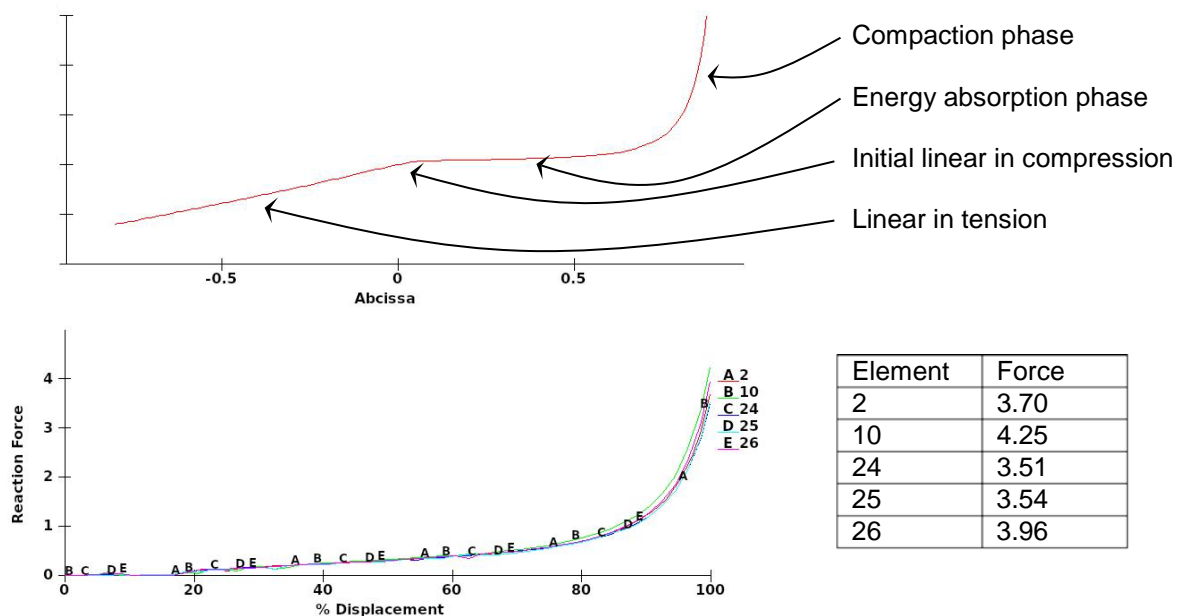
Figure 9 Input (compressive nominal) stress vs strain curve (top) and resulting reaction force of the indenter (bottom).

This material is highly compressible, whence the $\bar{B}$ method is not applied but all elements are fully integrated. Five simulations were conducted with the elements in the foam consisting of solid element

types 2 (fully integrated linear hexahedron), 10 (linear tetrahedron), 24 (fully integrated quadratic hexahedron), 25 (fully integrated pentahedron) and 26 (fully integrated tetrahedron). The mesh for the different inputs were targeted to make the number of nodes approximately the same, realized by using twice as many elements along each side of the foam block for the linear element inputs. The resulting reaction force curves are shown in Figure 9 together with a table with the final force values. Without drawing definite conclusions, it appears that the quadratic elements tend to be generally softer and the tetrahedral elements suffer from a stiffer response, although the differences are probably statistically insignificant.

Table 1 Statistics from nonlinear implicit solver for the foam test.

Element	Simulation time	Number of iterations	Number of residuals
2	672	348	1481
10	414	209	704
24	894	364	1507
25	723	258	950
26	982	367	1638

A full Newton method was used to solve the problems in approximately 50 steps; no retries were reported except for once in the solid element 2 simulation. Some statistics are shown in Table 1, that indicates an overall similar performance. Worth mentioning is that the global stiffness matrix for high order elements has a larger bandwidth for the same number of degrees of freedom, which will affect the time for solving the linear systems of equations, which may explain the lack of correlation between the simulation time and the number of iterations/residual evaluations.
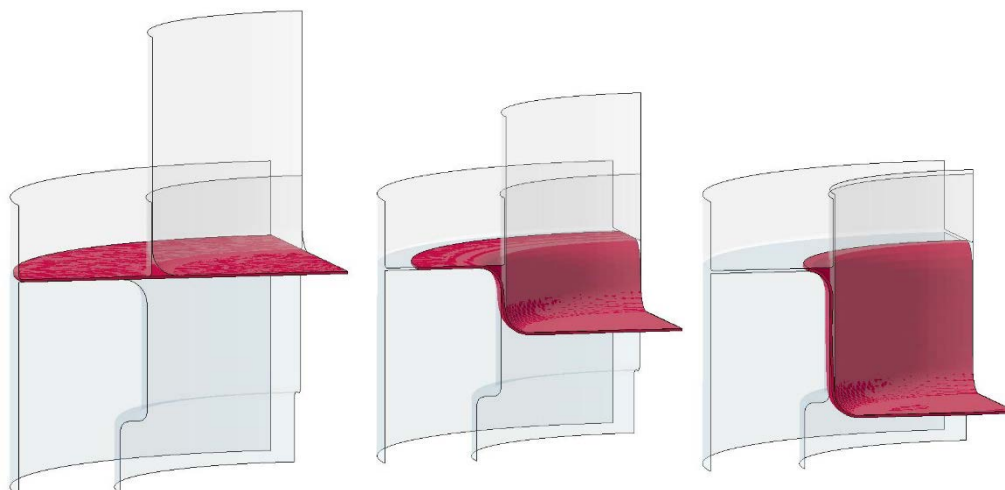
Figure 10 Deep draw, quarter model.

3.3 Deep Draw

A final example is the deep draw depicted in Figure 10. The setup is simple, a circular thin sheet is used with an isotropic elastic plastic material. Four different element types were used for the blank; the fully integrated quadratic solid element (type 24) with one element through the thickness, a linear solid element (type -2) with two elements through the thickness, the quadratic triangular shell (type 24 with locking treatment) and a low order quadrilateral shell (type 16). All different configurations use roughly the same number of nodes in the plane of the sheet to render an approximate similarity in model size. The solid elements have an aspect ratio of 1:5 and the results will be an indication of the consequences of modelling thin structures with high order solids, and also of using few elements through the thickness. The shell elements were included for contributing to the general discussion of results.

Table 2 Statistics from nonlinear solver for the deep draw.

Element	Number of stiffness ref.	Number of iterations	Number of residuals
Solid 24	460	4545	30957
Solid -2	138	2270	9376
Shell 24	118	1863	6597
Shell 16	62	1582	3568

In Figure 11 the punch force is shown, from which it seems that the shell elements provide a somewhat softer compared to the solid counterparts. No significant difference between the two solid elements, as between the two shell elements, is observed. The maximum plastic strain is between 43% and 44% in all simulations. From Table 2 we see that the high order solid is not converging at a plausible rate when compared to the other elements, which may be something to address in the future. A good explanation to this behaviour cannot be provided at the moment.
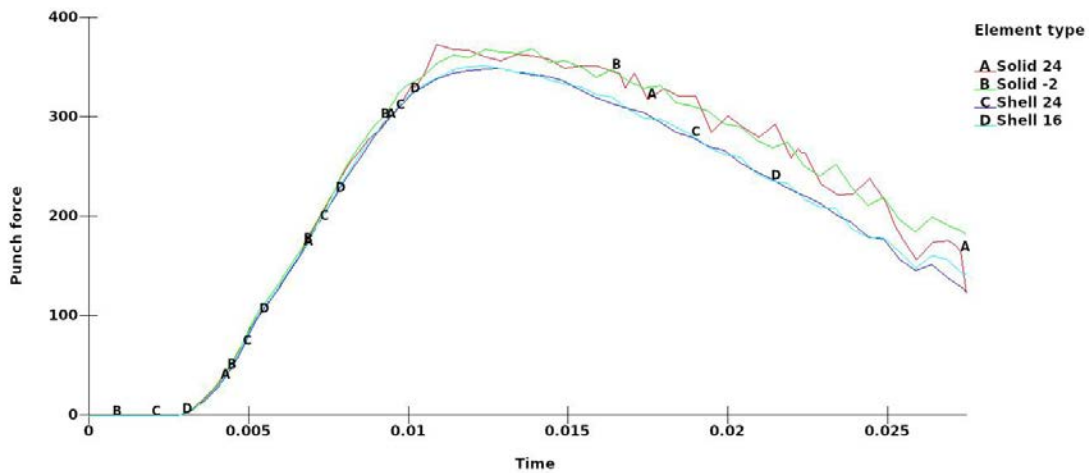
Figure 11 Punch force for the different setups.
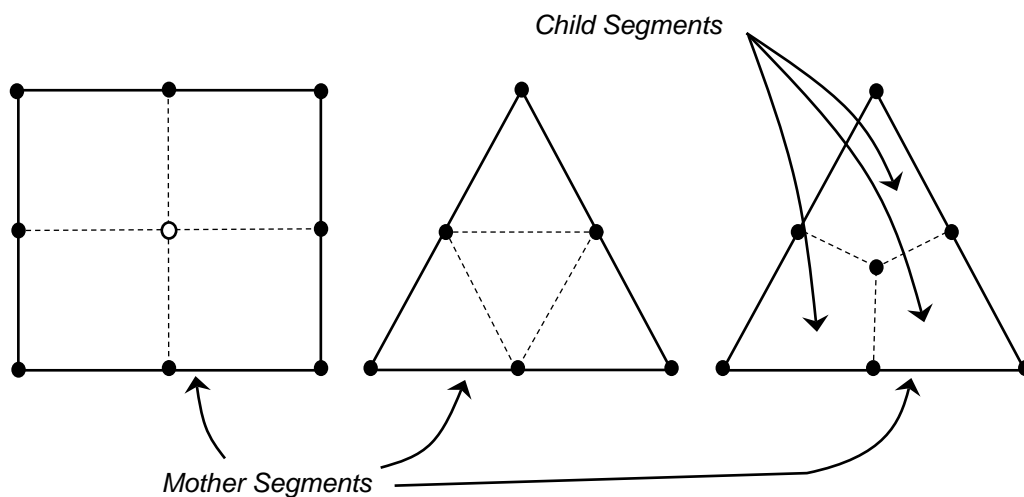
Figure 12 Segment partitioning of contact segments for contact kinematics, 8/9 noded segment, 6 noded segment and 7 noded segment, respectively.

4 Contacts

For contact between high order segments, or low order segments for that matter, the treatment should incorporate the underlying shape functions to yield nodal force consistency. For the Mortar contact, all linear and quadratic elements are accounted for in the sense of the following brief outline.

4.1   Kinematics

Obviously surfaces of high order elements are in general curved, which should be accounted for when computing the kinematics (i.e., the penetration and sliding) for the contact. For a segment to segment contact such as Mortar, the complexity and presumable cost to actually calculate and process the penetrated surface has lead us to take a simplified approach. To this end, a high order *mother-segment* are divided into 3 or 4 low order *child-segments* according to Figure 12. For 8 noded segments, i.e., those segments associated with the serendipity hexahedrals and quadrilaterals, a virtual node is created at the isoparametric center of the segment to aid in creating the 4 child-segments in this special case. This node is indicated by a circle in the figure. Then pairs of child-segments are used for computing the penetration field, and thus some second order geometry information is lost in the process.

4.2   Kinetics

The contact stress is evaluated according to the constitutive law for the contact, usually a standard Coulomb friction law, after which the virtual work principle is used to distribute the nodal forces. Here contact stress on a child-segment will result in nodal forces on *all* nodes of the mother segment. This will provide a correct nodal force distribution for a flat geometry, while the loss in accuracy for a curved geometry is hopefully compensated by increased efficiency and facilitated code maintenance. Furthermore, considering future development, incorporating cubic and isogeometric elements into the scheme becomes less complicated.

5 Summary

An overall trend in simulation technology is towards increasing the accuracy of model features to yield a more rapid convergence with mesh refinement. In the context of element technology, migrating from shells to solids or from low to high order elements are possible ways to accomplish this. This is particularly true for implicit analysis, where spatial discretization is limited by algorithmic complexity and memory consumption. Sometimes simulation standards and company regulations even make quadratic elements mandatory, and by tradition they are an important contribution to an implicit finite element software.

This has been a surficial overview of the quadratic elements available in LS-DYNA, with emphasis on implicit analysis. The element library is fairly complete, with the exception of a missing serendipity pentahedron which is expected to be added in the future. As shown in the examples, the available elements deliver what is promised; a response that is less prone to the known locking anomalies in finite element theory. Worth mentioning is the introduction of a new high order triangle that appear comparable to that of low order quadrilaterals, *and that will become available in version R11*. Regarding the overall implicit performance, this is the first study of its kind and results indicate good hopes for the future use of these elements.

6 Literature

[1]   LS-DYNA User's Keyword Manual Vol I-II, LSTC, 2017.

[2]   Hughes T.J.R., The Finite Element Method, Prentice-Hall, 1987.

[3]   Martin C.W., Breiner D.M. and Gupta K.K., A Six-Node Curved Triangular Element and a Four-Node Quadrilateral Element for Analysis of Laminated Composite Aerospace Structures, Technical report, NASA/CR-2004-210725, 2004.